

Various scenarios of metal-insulator transition in strongly correlated materials

J. Kuneš¹ and V. I. Anisimov^{2,*}

¹ Institute of Physics, Academy of Sciences of the Czech Republic, Cukrovarnická 10, 162 53 Praha 6, Czech Republic

² Institute of Metal Physics, Russian Academy of Sciences – Ural Division, 620041 Yekaterinburg GSP-170, Russia

Received 13 February 2011, revised and accepted 7 April 2011

Published online 13 September 2011

Key words Metal-insulator transition, dynamical mean-field theory, high-spin–low-spin transition.

This article is dedicated to Dieter Vollhardt on the occasion of his 60th birthday.

We review our investigations of electronic properties of strongly correlated materials using the combination of first principles electronic band structures and the dynamical mean-field theory, so called LDA+DMFT method. Our investigations focus on two phenomena, the spin state transitions and their relationship to the metal-insulator transition, and the effect of hybridization between correlated and ligand orbitals in charge-transfer type materials. The pressure driven spin transitions are studied for a group of materials containing MnO, FeO and Fe₂O₃. To investigate the hybridization effects we focus on NiO and NiS(Se)₂. We identify various mechanisms of the metal-insulator transition, which can take place in multi-band systems, in addition to the band-width control known from the single band Hubbard model.

© 2011 WILEY-VCH Verlag GmbH & Co. KGaA, Weinheim

1 Introduction

The effect of electron-electron interaction on the physical properties of materials has been one of the central questions of solid state physics since the early observation of the surprising properties of materials with incompletely filled *3d*-shells pointed out by de Boer and Verwey [1]. Over half a century long evolution lead to the current paradigm for understanding the materials with strong electronic correlations, the Hubbard model. It is only the last decade that the Hubbard model has been used in material specific studies. This development was enabled by the advances in numerical techniques for solution of quantum impurity problems, but most of all by development of the dynamical mean-field theory (DMFT) [2], which allowed the mapping of the lattice model onto a quantum impurity while preserving one of the most important dynamical features, the on-site correlation.

The early success of DMFT was marked by the description of the metal-insulator transition in the single-band Hubbard model at half-filling, controlled by the ratio of the interaction strength to the bare bandwidth U/W [3]. Yet, real materials have rarely only one active orbital per atom. More often they involve effects such as crystal-field splitting, Hund's rule coupling, hybridization to ligand-orbitals, or Fermi surface nesting [4]. These additional effects and the related degrees of freedom offer a broad range of possible parameters, which control the metal-insulator transition. It is the aim of this review to demonstrate this variety on the examples of materials we have studied using the DMFT approximation.

The paper is structured as follows. After a brief description of the computational method we investigate the relationship between the spin transition and the metal-insulator transition in simple oxides MnO, FeO,

* Corresponding author E-mail: via@imp.uran.ru

and Fe_2O_3 under applied pressure. Although in all three cases the ambient pressure phase corresponds to a high-spin insulator the materials behave differently. The main control parameter in these cases appears to be the crystal field splitting (and the bandwidth to some extent). In the second part of the results we focus on the role of hybridization in insulators. We present the results for the charge-transfer systems NiO and $\text{NiS}_{2-x}\text{Se}_x$. These provide yet another example of possible mechanism of metal-insulator transition.

2 Computational method

Our calculations proceed in two steps: (i) construction of the effective Hamiltonian from a converged LDA calculation, and (ii) solution of the corresponding DMFT equations, usually called the LDA+DMFT approach. [5] Here we express the Hamiltonian in the Wannier basis [7], which in the studied case consists of the interacting transition-metal d orbitals and non-interacting ligand p -orbitals

$$H = \sum_{\mathbf{k}, \sigma} (h_{\mathbf{k}, \alpha\beta}^{dd} d_{\mathbf{k}\alpha\sigma}^\dagger d_{\mathbf{k}\beta\sigma} + h_{\mathbf{k}, \gamma\delta}^{pp} p_{\mathbf{k}\gamma\sigma}^\dagger p_{\mathbf{k}\delta\sigma} + h_{\mathbf{k}, \alpha\gamma}^{dp} d_{\mathbf{k}\alpha\sigma}^\dagger p_{\mathbf{k}\gamma\sigma} + h_{\mathbf{k}, \gamma\alpha}^{pd} p_{\mathbf{k}\gamma\sigma}^\dagger d_{\mathbf{k}\alpha\sigma}) + \sum_{i, \sigma, \sigma'} U_{\alpha\beta}^{\sigma\sigma'} n_{i\alpha\sigma}^d n_{i\beta\sigma'}^d. \quad (1)$$

Here $d_{\mathbf{k}\alpha\sigma}$ and $p_{\mathbf{k}\gamma\sigma}$ are Fourier transforms of $d_{i\alpha\sigma}$ and $p_{i\gamma\sigma}$, which annihilate the d or p electron with orbital and spin indices $\alpha\sigma$ or $\gamma\sigma$ in the i th unit cell, and $n_{i\alpha\sigma}^d$ is the corresponding occupation number operator. The elements of $U_{\alpha\beta}^{\sigma\sigma'}$ matrix are parameterized in the usual way by U and J as described in [6]. To account for the Coulomb interaction already present in LDA we renormalize the dd -diagonal elements of the LDA Hamiltonian by the double counting correction

$$h_{\mathbf{k}, \alpha\beta}^{dd} = \tilde{h}_{\mathbf{k}, \alpha\beta}^{dd}(\mathbf{k}) - (N_{\text{orb}} - 1)\bar{U}n_d\delta_{\alpha\beta} \quad (2)$$

where n_d is the average d occupation per orbital and $N_{\text{orb}} = 10$ is the total number of orbitals within the shell.

Next we iteratively solve the DMFT equations on the Matsubara contour, a key part of which is the auxiliary impurity problem solved by the quantum Monte-Carlo (QMC) method. We have employed the Hirsch-Fye QMC [8] in the earlier works (NiO, MnO) and the strong-coupling continuous time QMC [9] (CT-QMC) in the more recent ones. We have checked the consistency by reproducing some of the Hirsch-Fye results with CT-QMC. To obtain the single-particle spectral functions analytic continuation to real frequencies is performed using the maximum entropy method [10].

3 Spin transitions in transition-metal oxides

Many compounds classified as Mott insulators exhibit large local moments which fulfill the first Hund's rule for the corresponding partial filling of the d shell, so called high spin (HS) state. Application of a sufficiently large pressure leads to destruction of the HS state and transition to a low spin (LS) state or a state without local moment. The HS-LS transition can be accompanied by an insulator-to-metal transition. We have investigated the relationship of these processes in several simple transition-metal oxides addressing the hen-and-egg question. All three materials MnO, Fe_2O_3 and FeO are characterized by octahedral coordination of the TM ions (with small distortion in Fe_2O_3) which gives rise to the pressure dependent e_g - t_{2g} splitting. MnO and Fe_2O_3 share the same local d^5 configuration of the TM ions, while FeO has a formal d^6 configuration.

3.1 Fe₂O₃

At ambient conditions, Fe₂O₃ is an antiferromagnetic (AFM) insulator ($T_N = 956$ K) with the corundum structure [11]. Photoemission spectroscopy (PES) at zero pressure [12] classified Fe₂O₃ as a charge-transfer insulator with the charge gap of 2.0–2.7 eV, inferred from the electrical conductivity data [13]. Under pressure, a first-order phase transition is observed at approximately 50 GPa (82% of the equilibrium volume) with the specific volume decreasing by almost 10% and the crystal symmetry being reduced (to the Rh₂O₃-II structure) [14]. The high-pressure phase is characterized by a metallic conductivity and the absence of both magnetic long-range order and the HS local moment.

Using LDA+DMFT calculations [15] we have found a first-order HS-LS transition with the local spin moment dropping from $\sim 4.5\mu_B$ to $\sim 1\mu_B$. In Fig. 2 we show the evolution of the one-particle spectra, which exhibits a gap in the HS phase and a metallic LS phase. Increasing the pressure within the HS phase has two effects: (i) an increase of the crystal-field splitting between the e_g and t_{2g} peaks (well visible in both upper and lower Hubbard bands), (ii) band broadening. Both these effects lead to continuous squeezing of the gap down to zero. Once the gap disappears electronic reconstruction takes place and the system flips into a LS state with lower kinetic energy. The volume collapse can be understood as a consequence of emptying of the anti-bonding e_g bands.

3.2 MnO

MnO crystallizes in the rock-salt structure and exhibits AFM order below 118 K. The shock data [16], and later Raman and optical studies [17], had identified a transformation in MnO in the neighborhood of 90–105 GPa. Transport [18], magnetic, structural and spectroscopic [19], and reflectivity [17] data all point to a first-order, insulator-metal Mott transition near 100 GPa with volume ($v = V/V_0$) collapse $v = 0.68 \rightarrow 0.63$, and moment collapse (from $\sim 5\mu_B$ to $1\mu_B$ or less [19]). The structural data indicate a B1 \rightarrow B8 change just before the Mott transition, which thus occurs within the B8 (NiAs) phase rather than the B1 (NaCl) phase.

The LDA+DMFT calculations performed in the rock-salt structure found a continuous HS-LS crossover as a function of volume. Investigating the total energy, however, revealed a discontinuous volume change comparable to the experimentally observed one [20]. In Fig. 1 we show the evolution of the one-particle

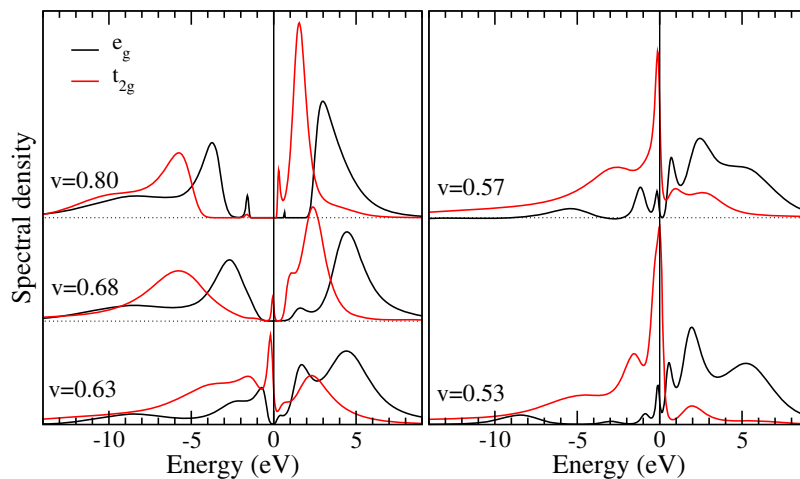


Fig. 1 (online colour at: www.ann-phys.org) The one-particle spectra of MnO at various specific volumes ($T = 1160$ K) in the vicinity of the spin transition. The Mn d spectra are resolved into the e_g and t_{2g} contributions, O p spectra are not shown.

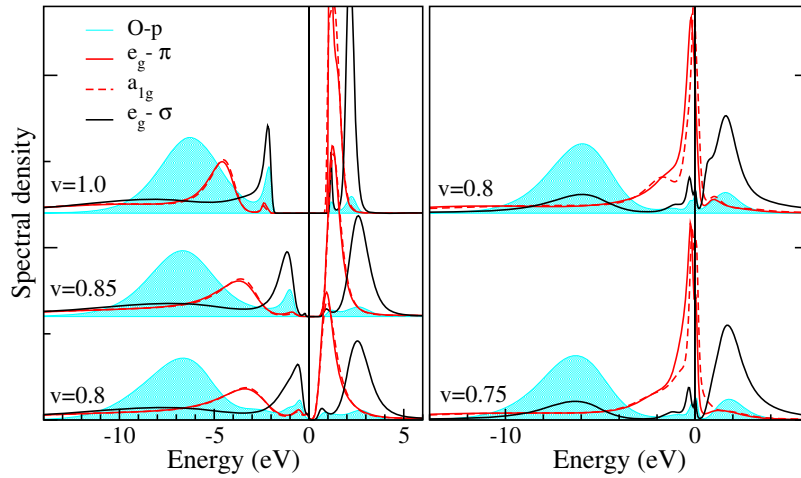


Fig. 2 (online colour at: www.ann-phys.org) The single-particle spectra of Fe_2O_3 at various specific volumes ($T = 580$ K). The HS solutions are shown in the left and LS solutions in the right panel. The Fe d spectra are resolved into the e_g (called e_g^σ in the legend) and t_{2g} (further split in a_{1g} and e_g^π by distortion from precise octahedral symmetry) contributions. The O p spectra are marked by blue shading.

spectra corresponding to Mn- $3d$ orbitals. The HS spectra of MnO resembles that of Fe_2O_3 including the reduction of the gap with pressure. Also the LS spectra of the two iso-electronic materials look similar. However, the HS-LS transition in MnO proceed quite differently from Fe_2O_3 . In particular, before the gap between the e_g valence band and t_{2g} conduction band may be squeezed to zero the local moment starts to dwindle and simultaneously in-gap states of t_{2g} character appear. We attribute this behavior to the on-site competition between the Hund's rule (favoring HS state) and the crystal-field splitting (favoring LS state). A detailed discussion and comparison to model calculations of Werner and Millis [21] can be found in [22].

3.3 FeO

FeO also becomes metallic under high pressure. Resistivity measurements showed that FeO becomes metallic at pressures exceeding 72 GPa [23]. At ambient conditions FeO has cubic rock-salt B1 structure [24]. It orders anti-ferromagnetically below $T_N = 198$ K. Under pressure at room temperature rhombohedral distortion accompanying the AFM order is observed at ≈ 15 GPa and this structure is preserved up to at least 140 GPa [25]. In contrast to MnO and Fe_2O_3 presence of HS-LS transition in FeO is controversial. Mössbauer spectroscopy [26] shows that quadrupole splitting appears between 60 and 90 GPa, which was interpreted as a signature of LS diamagnetic state. On the other hand high pressure X-ray emission spectroscopy [27] demonstrates that the satellite feature in Fe $K\beta$ line associated with HS Fe^{2+} state does not disappear up to 143 GPa. Note, that accurate treatment of Mössbauer data [27] confirms the absence of HS-LS transition.

In FeO LDA+DMFT results [28] reveal yet another behavior shown in Fig. 3. Namely an orbital selective insulator-to-metal transition is found without a spin transition. Essentially the transition proceeds by squeezing of the gap due crystal-field splitting and band broadening like in Fe_2O_3 . However, since the gap has a t_{2g} - t_{2g} character its closing does not involve changes in orbital occupancy and thus the spin transition is missing. The difference between the HS valence-band spectra of d^5 and d^6 ions, in particular the two peaks in the t_{2g} channel, can be easily understood on ionic level. Starting from d^6 $S = 2$ state and emitting a t_{2g} electron one can reach either $S = 5/2$ final state (low energy peak) or $S = 3/2$ final state (high energy peak). By emitting an e_g electron only $S = 3/2$ final state can be reached, which has an energy between the states reached by t_{2g} emission.

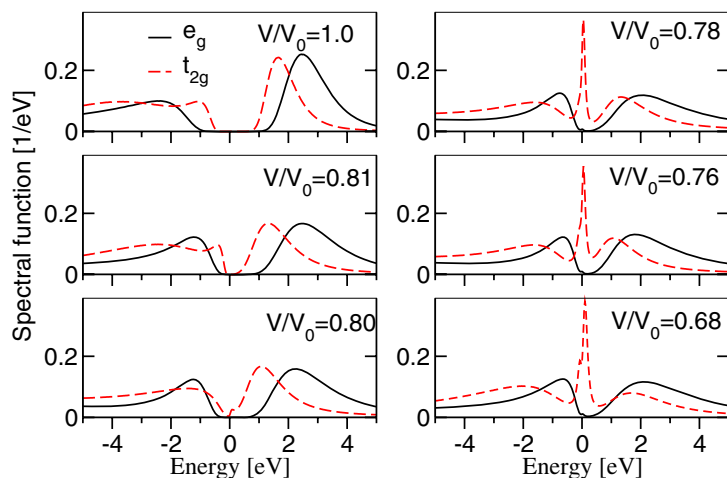


Fig. 3 (online colour at: www.ann-phys.org) Spectral function of Fe-d states in FeO vs. pressure obtained in LDA+DMFT (CT-QMC) calculations at room temperature.

4 Mott transition in charge-transfer systems

Zaanen, Sawatzky and Allen [29] introduced the name charge-transfer insulators for a class of Mott insulators with the property that added electrons reside on the TM atoms while added holes reside on the ligand atoms, cuprate perovskites being a notorious example. Here we address the physics of another classic charge-transfer insulator NiO and its electronic analogs NiS₂ and NiSe₂. The interest in NiS_{2-x}Se_x solid solutions arises from the metal-insulator transition, which they exhibit as a function of Se concentration x or applied pressure.

NiX₂ ($X = S, Se$) can be viewed as NiO with the O atom replaced by an X₂ dimer, which accommodates two holes in its p_{σ}^* anti-bonding orbital leading to an X₂⁻² valence state. The analogy is supported by numerous photoemission studies [30]. The LDA+DMFT spectra [31, 32], which capture quite well the experimental features, are shown in Fig. 4. The first interpretation of the one-particle spectra of NiO was based on small cluster exact diagonalization studies [33]. Multiple peaks in the valence part of the spectral function of both e_g and t_{2g} electrons, arising from combination of the p - d hybridization and the electronic correlation in the Ni d shell, appear in all three materials. Also the two-peak feature in the e_g conduction band spectrum of NiS₂ has the same origin.

The central question concerning NiS_{2-x}Se_x is: why is NiS₂ an insulator while NiSe₂ is metallic? Several proposals appear in the literature: (i) larger d -band width in NiSe₂, (ii) overlap of the Se- p with the upper Hubbard band in NiSe₂, (iii) smaller interaction strength U due to a large polarizability of the Se-Se dimer. Our calculations [32] suggest that none of these scenarios actually takes place. As for (i), besides the fact that the d -bandwidth is not a particularly meaningful quantity in CT systems, the d peaks in the LDA as well as the LDA+DMFT spectra are narrower in NiSe₂. The scenario (ii) is excluded as the upper Hubbard band, which corresponds to the 3.5 eV peak in NiS₂ is not the lowest electron-addition excitation of NiS_{2-x}Se_x. And finally proposal (iii) is ruled out since the presence or absence of the gap in the spectra of NiS₂ and NiSe₂ does not depend on the U value within the studied range of 4.5–7 eV (the calculated U value is ~ 5 eV). Our interpretation of the metal-insulator transition is based on the observation that the lowest electron-addition energy is determined by the position of the S-S (Se-Se) dimer anti-bonding state, i.e. it reflects the bonding strength (bonding–anti-bonding splitting) in the dimer. A weaker bonding in Se-Se dimer leads to the overlap of the dimer anti-bonding band with the valence band and thus causes the disappearance of the gap. The pressure induced metal-insulator transition can be understood

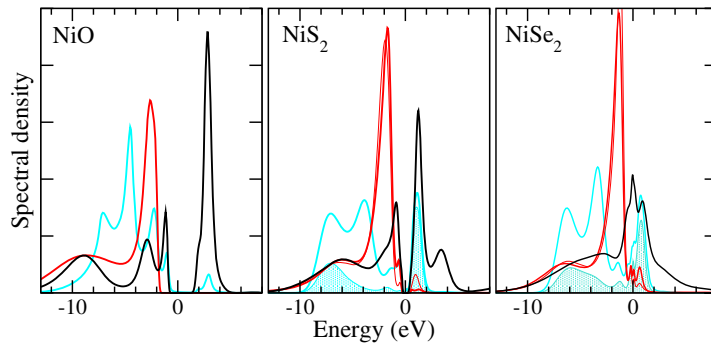


Fig. 4 (online colour at: www.ann-phys.org) The single-particle spectra of NiO, NiS₂ and NiSe₂ resolved into the Ni-d e_g (black) and t_{2g} (red) as well as the ligand (blue) contributions. The blue shading corresponds to the orbitals forming the dimer σ -bond in NiS₂ and NiSe₂.

as follows. While the S-S bonding–anti-bonding splitting remains constant, since the dimer behaves as a rigid object, reduction of the inter-dimer distances leads to an overall broadening of the S- p bands as well as an increased p - d hybridization. These effects lead to the closing of the gap as shown by explicit calculations [32].

5 Conclusions

Using several examples we have demonstrated that combination of DMFT with band structures of real materials leads to numerous possibilities for metal-insulator transition, which cannot be realized in simple models. We have presented examples where MIT takes place simultaneously with spin transition, MnO and Fe₂O₃, as well as FeO where MIT takes place without significant reduction of the large local moment. On the example NiS_{2-x}Se_x we have demonstrated a mechanism controlling MIT, which was not proposed previously and which requires explicit inclusion of the ligand bands into the effective Hamiltonian.

Acknowledgements The authors thank A. O. Shorikov, S. L. Skornyakov, Dm. M. Korotin, P. Werner, A. V. Lukoyanov, R. T. Scalettar and W. E. Pickett for collaboration on reviewed works. This work was supported by grant No. P204/10/0284 of the Grant Agency of the Czech Republic and by the Deutsche Forschungsgemeinschaft through FOR 1346, by the Russian Foundation for Basic Research Project Nos. 10-02-00046a, the fund of the President of the Russian Federation for the support of scientific schools NSH 4711.2010.2, the Program of the Russian Academy of Science Presidium “Quantum microphysics of condensed matter” N7, Russian Federal Agency for Science and Innovations (Program “Scientific and Scientific-Pedagogical Trained of the Innovating Russia” for 2009–2010 years), grant No. 02.740.11.0217, the scientific program “Development of Scientific Potential of Universities” No. 2.1.1/779.

References

- [1] J. H. de Boer and E. J. W. Verwey, Proc. Phys. Soc. **49**(4S), 59 (1937); N. F. Mott, Proc. Phys. Soc. **49**(4S), 57 (1937).
- [2] W. Metzner and D. Vollhardt, Phys. Rev. Lett. **62**, 324 (1989); A. Georges and G. Kotliar, Phys. Rev. B **45**, 6479 (1992); G. Kotliar and D. Vollhardt, Phys. Today **57**(3), 53 (2004).
- [3] A. Georges, G. Kotliar, W. Krauth, and M. J. Rozenberg, Rev. Mod. Phys. **68**, 13 (1996).
- [4] E. Pavarini et al., Phys. Rev. Lett. **92**, 176403 (2004).
- [5] K. Held et al., Phys. Status Solidi B **243**, 2599 (2006); G. Kotliar et al., Rev. Mod. Phys. **78**, 865 (2006).
- [6] A. I. Liechtenstein, V. I. Anisimov, and J. Zaanen, Phys. Rev. B **52**, R5467 (1995).
- [7] V. I. Anisimov et al., Phys. Rev. B **71**, 125119 (2005).

- [8] J. E. Hirsch and R. M. Fye, *Phys. Rev. Lett.* **56**, 2521 (1986).
- [9] P. Werner, *Phys. Rev. Lett.* **97**, 076405 (2006).
- [10] M. Jarrell and J. E. Gubernatis, *Phys. Rep.* **269**, 133 (1996).
- [11] C. G. Shull, W. A. Strauser, and E. O. Wollan, *Phys. Rev.* **83**, 333 (1951).
- [12] A. Fujimori, *Phys. Rev. B* **34**, 7318 (1986); C.-Y. Kim et al., *Phys. Rev. B* **66**, 085115 (2002); R. J. Lad and V. E. Henrich, *Phys. Rev. B* **39**, 13478 (1989).
- [13] S. Mochizuki, *Phys. Status Solidi A* **41**, 591 (1977); K.-H. Kim, S.-H. Lee, and J.-S. Choi, *J. Phys. Chem. Solids* **46**, 331 (1985).
- [14] M. P. Pasternak et al., *Phys. Rev. Lett.* **82**, 4663 (1999); G. Kh. Rozenberg et al., *Phys. Rev. B* **65**, 064112 (2002); H. Liu et al., *Phys. Chem. Miner.* **30**, 582 (2003).
- [15] J. Kuneš et al., *Phys. Rev. Lett.* **102**, 146402 (2009).
- [16] Y. Noguchi, K. Kusaba, K. Fukuoka, and Y. Syono, *Geophys. Res. Lett.* **23**, 1469 (1996).
- [17] Y. Mita et al., *Phys. Status Solidi B* **223**, 247 (2001); Y. Mita, D. Izaki, M. Kobayashi, and S. Endo, *Phys. Rev. B* **71**, 100101 (2005).
- [18] J. R. Patterson et al., *Phys. Rev. B* **69**, 220101 (2004).
- [19] C. S. Yoo et al., *Phys. Rev. Lett.* **94**, 115502 (2005); J.-P. Rueff et al., *J. Phys.: Condens. Matter* **17**, S717 (2005).
- [20] J. Kuneš et al., *Nature Mater.* **7**, 198 (2008).
- [21] P. Werner and A. J. Millis, *Phys. Rev. Lett.* **99**, 126405 (2007).
- [22] J. Kuneš et al., *Eur. Phys. J., Spec. Top.* **180**, 5 (2010).
- [23] E. Knittle, R. Jeanloz, A. C. Mitchel, and W. J. Nellis, *Solid State Commun.* **59** 513 (1986).
- [24] B. T. M. Willis and H. P. Rooksby, *Acta Crystallogr.* **6**, 827–831 (1953).
- [25] T. Yagi, T. Suzuki and S. Akimoto, *J. Geophys. Res. B* **90**, 8784 (1985); S. Ono, Y. Ohishi, and T. Kikegawa, *J. Phys.: Condens. Matter* **19**(3), 036205 (2007).
- [26] M. P. Pasternak, *Phys. Rev. Lett* **79**, 5046 (1997).
- [27] J. Badro et al., *Phys. Rev. Lett* **83**, 4101 (1999).
- [28] A. O. Shorikov, *Phys. Rev. B* **82**, 195101 (2010).
- [29] J. Zaanen, G. A. Sawatzky, and J. W. Allen, *Phys. Rev. Lett.* **55**, 418 (1985).
- [30] E. K. Li, K. H. Johnson, D. E. Eastman, and J. L. Freeouf, *Phys. Rev. Lett.* **32**, 470 (1974); W. Folkerts et al., *J. Phys. C* **20**, 4135 (1987); A. Fujimori et al., *Phys. Rev. B* **54**, 16329 (1996).
- [31] J. Kuneš, V. I. Anisimov, A. V. Lukoyanov, and D. Vollhardt, *Phys. Rev. B* **75**, 165115 (2007); J. Kuneš et al., *Phys. Rev. Lett.* **99**, 156404 (2007).
- [32] J. Kuneš et al., *Phys. Rev. B* **81**, 035122 (2010).
- [33] A. Fujimori, F. Minami, and S. Sugano, *Phys. Rev. B* **29**, 5225 (1984); G. A. Sawatzky and J. W. Allen, *Phys. Rev. Lett.* **53**, 2339 (1984).